Multifragmentation in the 4.8-GeV ^{3}He + ^{nat}Ag, ^{197}Au Reactions

K. Kwiatkowski,[1] K. B. Morley,[1] E. Renshaw Foxford,[1] D. S. Bracken,[1] V. E. Viola,[1] N. R. Yoder,[1] R. Legrain,[2] E. C. Pollacco,[2] C. Volant,[2] W. A. Friedman,[3] R. G. Korteling,[4] J. Brzychczyk,[5] and H. Breuer[6]

[1]*Department of Chemistry and Physics and IUCF, Indiana University, Bloomington, Indiana 47405*
[2]*Commissariat à l'Energie Atomique DAPNIA/Service de Physique des Particles, Centre d'Etudes de Saclay, 91191 Gif-sur-Yvette Cedex, France*
[3]*Department of Chemistry, Simon Fraser University, Burnaby, British Columbia, Canada V5A 1SG*
[4]*Department of Physics, University of Wisconsin, Madison, Wisconsin 53706*
[5]*Institute of Physics, Jagiellonian University, 30-059 Krakow, Poland*
[6]*Department of Physics, University of Maryland, College Park, Maryland 20742*

(Received 11 October 1994)

Multifragmentation of ^{nat}Ag and ^{197}Au nuclei induced by a 4.8-GeV ^{3}He ions has been studied with the Indiana Silicon Sphere 4π detector array. Rapidity and moving source analyses are consistent with thermal emission from a source in approximate kinetic equilibrium. For the most dissipative collisions, the spectral Coulomb peaks are broadened to very low energies, indicative of emission from an extended nuclear system. Predictions of a model with an intranuclear cascade and an expanding, emitting source compare well with experimental multiplicity distributions and the evolution of fragment spectral shapes.

PACS numbers: 25.55.–e, 25.70.Pq

When nuclei are subjected to extreme conditions of thermal or compressional energy, multifragmentation occurs with high probability [1–7]. The nature of this disintegration process may provide insight into the nuclear equation of state at low densities, limiting temperatures in the nuclear medium, and the possibility of a liquid-gas phase transition in finite nuclei. A related important question is the role of nuclear expansion in the breakup process. Analysis of recent exclusive data [2,6,8–10] suggests that multifragmentation occurs from an extended nuclear system, corresponding to relatively low densities ($\rho/\rho_0 \sim 1/3$). Direct experimental evidence for this behavior is presented in this Letter, based on the observed evolution of the fragment spectra as a function of collision violence.

Investigations of hot nuclei formed with light-ion beams (H and He) at energies above ~1 GeV are an important complement to studies with heavy-ion probes. For light-ion-induced reactions, the multifragmentation mechanism is driven by thermal heating and strongly influenced by the excitation of Δ resonances during the cascade, followed by rescattering and/or readsorption of the decay pions [9,11,12]. Light-ion beams also insure that energy dissipation occurs on a fast time scale (≤ 30 fm/c), permitting rapid destabilization of the system. Further, since compressional and rotational effects should be negligible, it becomes possible to isolate the thermal component of the multifragmentation process.

In this Letter, we report the first studies of light-ion-induced multifragmentation in which both light charged particle (LCP = H and He) and intermediate-mass fragments (IMF: $3 \leq Z \leq 20$) are fully Z identified with low thresholds and large solid angle coverage. The experiments were performed at the Saturne II accelerator at the Laboratoire National Saturne using the Indiana Silicon Sphere 4π detector array [13]. Beams at 4.8-GeV ^{3}He ions of intensity, i.e., $\sim 5 \times 10^7$/spill, were used to bombard targets of 1.0 mg/cm^2 ^{nat}Ag and 1.5 mg/cm^2 ^{197}Au. An active collimator system was used to minimize beam halo contributions.

The Indiana Silicon Sphere array consists of 162 detector telescopes, covering 14° to 86.5° and 93.5° to 166° in polar angle, giving a nominal coverage of 74% of 4π. Each telescope is composed of (1) a gas-ionization chamber operated at 17–18 Torr of C_3F_8 gas; (2) a 500 μm ion-implanted passivated silicon detector, and (3) a 28 mm thick CsI ($T\ell$) scintillator with photodiode readout. Detector identification thresholds (including target, window, and dead-layer thickness losses) were $E/A \sim 0.8$ MeV. The maximum telescope stopping power was $E/A = 96$ MeV. Fast signals from two or more silicon detectors provided a minimum bias trigger for the data acquisition system.

In Fig. 1, we compare the primary IMF multiplicity distributions for the 4.8-GeV ^{3}He + ^{nat}Ag and ^{197}Au systems reconstructed from a GEANT simulation [14] that includes detector geometry and experimental angular distributions. The IMF multiplicity for the ^{197}Au target extends to distinctly higher values than for ^{nat}Ag, roughly in proportion to the available mass for each system. For reconstructed events with at least one IMF, we find $\langle M_{\rm IMF}\rangle = 1.5$ for ^{nat}Ag and 2.0 for the ^{197}Au target for fully identified events. These values are similar to, although slightly lower than, those observed in heavy-ion reactions for similar total mass and bombarding energy [15]. They are much lower than the value of $\langle M_{\rm IMF}\rangle = 3.8$ previously reported by Lips *et al.* [16] for the comparable 4.0-GeV ^{4}He + ^{197}Au reaction. The

 0031-9007/95/74(19)/3756(4)$06.00

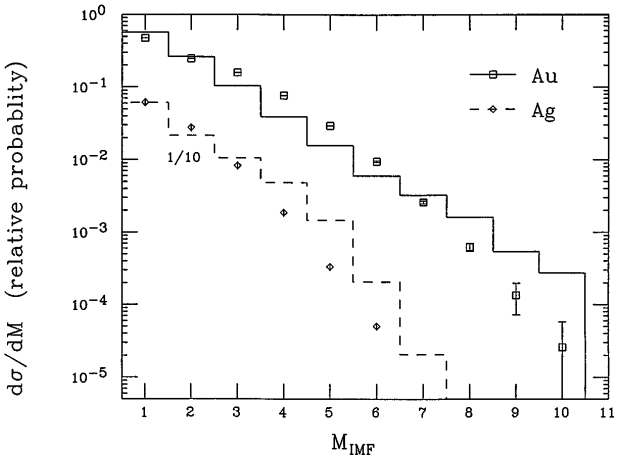

FIG. 1. Reconstructed multiplicity distributions for IMFs for 4.8-GeV ^{3}He bombardments of ^{nat}Ag and ^{197}Au targets. Histograms are predictions of INC-EES model [9].

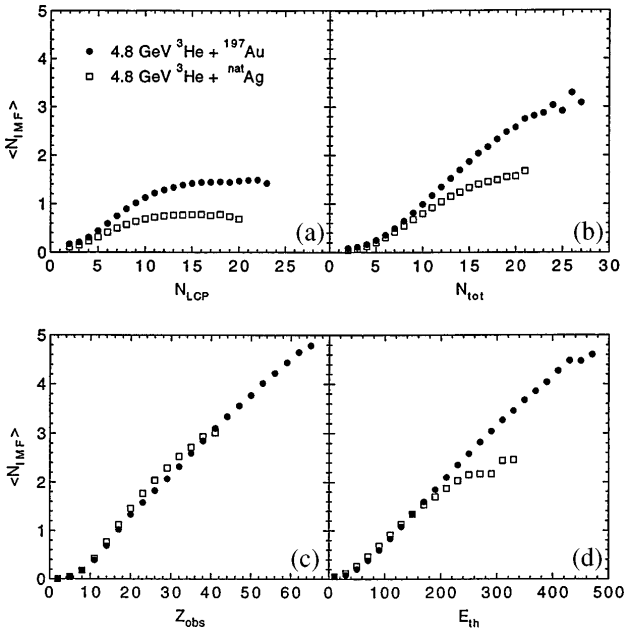

FIG. 2. Average IMF multiplicity $\langle N_{\mathrm{IMF}}\rangle$ plotted as a function of (a) light charged-particle multiplicity, N_{LCP}, (b) total charged-particle multiplicity N_{tot}, (c) total observed charge Z_{obs}, and (d) total thermal energy E_{th}, in MeV.

shapes of the multiplicity distributions in our work also differ significantly from Lips *et al.*

In order to compare with theories of multifragmentation, it is important to have an accurate gauge of the excitation energy distribution of the emitting source. All such theories [17] predict that the IMF multiplicity and excitation energy are strongly correlated. Under this assumption, the average observed IMF multiplicities $\langle N_{\mathrm{IMF}}\rangle$ have been plotted against several variables believed to be associated with energy deposition in the collision, as shown in Fig. 2. Among these are observed LCP multiplicity N_{LCP}, total charged-particle multiplicity N_{tot}, total observed charge Z_{obs}, and total thermalized energy E_{th}. We define the thermalized energy for each event to be the sum of fragment kinetic energies near the Coulomb peak ($E/Z \lesssim 25$ MeV); i.e., the preequilibrium tails of the spectra and fast leading particles are eliminated on the basis of slope changes in the spectral tails. The total thermalized energy scales directly with total transverse energy, commonly used in heavy-ion analyses.

When compared with total observed LCP multiplicities, $\langle N_{\mathrm{IMF}}\rangle$ becomes constant at large values of N_{LCP}, reaching saturation near $\langle N_{\mathrm{IMF}}\rangle \approx 0.75$ for ^{nat}Ag and 1.5 for ^{197}Au, roughly proportional to the target masses. This result is consistent with intranuclear cascade (INC) calculations, which predict only a weak positive correlation between the fast LCP multiplicity and large deposition energies due to the very large fluctuations during the cascade. A better correlation is obtained when the total charged-particle multiplicities are compared with $\langle N_{\mathrm{IMF}}\rangle$. For the most dissipative collisions, the maximum $\langle N_{\mathrm{IMF}}\rangle$ reaches values approximately twice as large as for LCP's alone (i.e., maxima of $\sim$1.5 for ^{nat}Ag and 3.0 for ^{197}Au). This result is similar to data from comparable systems in heavy-ion-induced reactions [6,15].

More sensitive correlations with IMF multiplicities are found for the total detected charge Z_{obs}, and the total thermalized energy E_{th}. Both ^{nat}Ag and ^{197}Au follow nearly identical behavior over the entire observed range in Z_{obs}, with a slope of approximately 12 charge units/IMF emitted, on average. Maximum $\langle N_{\mathrm{IMF}}\rangle$ values of 2.8 for ^{nat}Ag and 4.6 for ^{197}Au are found, in good agreement with INC–expanding-emitting-source calculations [9], discussed below. Since our detection system is not sensitive to very low energy heavy residues, Z_{obs} is approximately proportional to the number of participant protons in the fragmentation process. Thus, Z_{obs} should be directly related to the collision violence. The total thermalized energy should be an approximate measure of the excitation energy of the emitting source, when effects due to missing solid angle, neutron emission, and separation energies are taken into account. From Fig. 2 we conclude that the total observed charge and thermalized energy provide good measures of the energy dissipated by the beam into internal energy of the system.

In order to estimate the degree of equilibrium of the average multifragmentation source, rapidity analyses have been performed. To a good approximation, the data for any given IMF invariant cross section are isotropic, roughly independent of IMF multiplicity for $M_{\mathrm{IMF}} > 1$. This suggests that the system is in at least approximate kinetic equilibrium; i.e., the momentum distribution in the source is randomized, but not necessarily statistically equilibrated. Source velocities are ~ 0.01–$0.02c$, in good

agreement with moving-source fits and intranuclear cascade code predictions [18].

Moving source fits have also been performed for IMFs as a function of $Z_{\rm obs}$. Following procedures outlined in Ref. [19], the spectra are parametrized in terms of a slow and a fast source. The slow source, which is dominant, assumes surface emission from a nucleus with charge Z, velocity v, temperature T, fractional Coulomb barrier k_C, and Coulomb shape parameter p [20]. The fast source is a standard Maxwellian function. An important aspect of these fits is that the charge of the emitting source is taken as $Z_{\rm source} = Z_{\rm target} + Z_{\rm proj} + Z_{\rm IMF} - Z_{\rm obs}$; i.e., we assume all charge observed in the reaction is emitted *prior to* emission to the IMF. While this is an extreme assumption, it minimizes the calculated Coulomb repulsion between the fragment and its residue, and maximizes k_C. Least-squares fit parameters for the slow source are shown in Table I for carbon fragments.

Direct evidence for emission from an extended source is found in the behavior of the fractional Coulomb barrier k_C in Table I. For large $Z_{\rm obs}$ values we find that k_C decreases as a function of $Z_{\rm obs}$. In order to obtain an estimate of the breakup density for the ^{197}Au system, we compare values of k_C for the two extreme cases of $Z_{\rm obs}$. The former should approximate emission from a source at normal nuclear matter density and the latter from the extended source. This analysis yields a value of $\rho/\rho_0 \lesssim 1/3$ for the multifragmentation system. However, the geometry of the emitting source may also play an important role in a more quantitative analysis. The $^{\rm nat}$Ag system does not lend itself to a similar analysis because of the very low Coulomb peaks. This observation, plus the apparent isotropic nature of the source, is suggestive of significant energy deposition followed by nuclear expansion prior to fragment emission—or of some mechanism which is accompanied by a major disruption of the Coulomb field of the emitting source.

The temperature parameter T in Table I increases uniformly as a function of collision violence ($Z_{\rm obs}$), reaching values near $T \approx 18$ MeV. For the least violent collisions, the values of T are relatively low, comparable to nonequilibrium emission in lower energy ^{3}He-induced reactions [19].

TABLE I. Moving source fit parameters [19] for carbon fragments emitted in the 4.8-GeV ^{3}He + $^{\rm nat}$Ag, ^{197}Au reactions, as defined in the text.

$Z_{\rm obs}$ (Ag)	k_C	T (MeV)	$Z_{\rm obs}$ (Au)	k_C	T (MeV)
7–12	0.32	11.5	1–10	0.64	8.3
13–18	0.10	14.5	11–20	0.58	11.0
19–24	0.03	16.5	21–30	0.46	14.4
25–30	0.00	17.9	31–40	0.42	15.9
31–36	0.05	20.1	41–50	0.44	17.5
			51–60	0.44	18.8

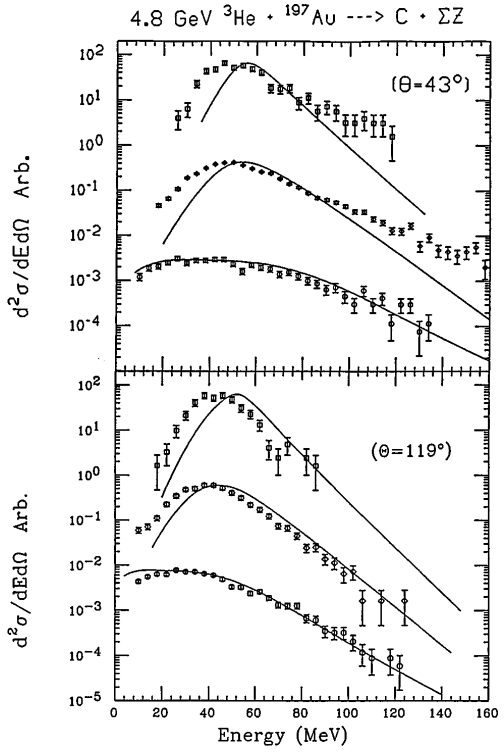

FIG. 3. Laboratory energy spectra of carbon fragments for the 4.8-GeV ^{3}He + ^{197}Au reaction, gated on total observed charge. Points are data for $Z_{\rm obs} = 1-10$ (top), $Z_{\rm obs} = 11-20$ (middle), and $Z_{\rm obs} = 41-50$ (bottom). Lines are predictions of the INC-EES model, as described in the text. Data and calculations are normalized so that maximum probabilities are equal in magnitude.

In Fig. 3 the energy spectra of carbon fragments, gated on $Z_{\rm obs}$ are shown. With increasing $Z_{\rm obs}$ bin, one observes a decrease in the Coulomb peak energy, a broadening of the peaks toward lower energies, and a systematic hardening of the high energy spectral slopes, consistent with the moving source parameters in Table I. This aspect of the data again emphasizes the strong distortion of the Coulomb field of the emitting source relative to emission from a spherical source at normal nuclear matter density.

These data have been compared with predictions based on a hybrid intranuclear-cascade-expanding-emitting-source (INC-EES) statistical model [9,19,21]. Excitation energy distributions from the INC calculation [18], binned in 100 MeV steps, along with the corresponding average values of the mass, charge, and velocity of the residue, provide input for the expanding emitting source calculations. In this model, IMF emission occurs sequentially, but on a fast time scale ($\lesssim$70 fm/c), during the expansion. If the thermal pressure is sufficient to reach nuclear densities of $\rho/\rho_0 \lesssim 0.3$, multifragmentation of the residue then occurs. At this point, surface fragment emission is replaced by volume emission in

calculating the fragment spectra. Volume emission may also be interpreted in terms of simultaneous breakup of the expanded reside. To examine this point, a sphericity (S) and coplanarity (C) event shape analysis [22] was found to yield a high degree of sphericity for the most dissipative events (e.g., $\langle S \rangle = 0.52$ and $\langle C \rangle = 0.15$ for $M_{\mathrm{IMF}} = 6$) for the ^{197}Au target.

The calculated multiplicity results are compared with the reconstructed data in Fig. 1. For ^{197}Au the calculation describes the data well for most of the IMF cross section. For $^{\mathrm{nat}}$Ag, the agreement is somewhat poorer, but may be improved by more exact treatment of detector thresholds in the simulation. In comparing the INC-EES model with the data, no attempt has been made to adjust the input parameters, which are identical for both targets and based on Ref. [9]. In this regard, it is worth noting the differences in excitation energy distributions predicted by the INC code. For ^{197}Au, initial excitation energies up to 1500 MeV, or $E^*/A \gtrsim 8.5$ are calculated for the most dissipative collisions, whereas for $^{\mathrm{nat}}$Ag, these values are 1000 MeV and $E^*/A \gtrsim 12$ MeV. Overall, the calculations and data are consistent only if expansion is included in the model.

Predictions of the spectral shapes by the INC-EES model are compared with the data in Fig. 3. The trends parallel one another well. Particular success is achieved in reproducing the data for large Z_{obs} values, where the model should be most appropriate. In terms of the model, the overall behavior can be explained as follows. The most energetic fragments are emitted early in the expansion from a high Z source near normal matter density; they also receive a boost in energy from the source expansion velocity. Since both the excitation energy and expansion velocity should scale with Z_{obs}, the spectral slopes are expected to become systematically flatter with increasing Z_{obs}. For systems that expand to the critical breakup density ($\rho/\rho_0 \sim 0.3$), the expansion velocity is near zero and the system is highly distended. Thus, fragments emitted at this stage experience greatly reduced Coulomb repulsion, resulting in very low energy fragments.

The poorest agreement in Fig. 3 is found for the lowest Z_{obs} bins. Fast processes [2,19] in more peripheral reactions may also contribute to the experimental spectra. Evidence for such a fast source is present elsewhere in the data (at the ~15% level), but is not discussed here. This mechanism is not included in the INC-EES model.

In conclusion, the 4.8-GeV ^{3}He + $^{\mathrm{nat}}$Ag and ^{197}Au reactions have been studied with a low threshold, large solid angle particle identification array. For these reactions, thermal heating is expected to be a major mechanism in producing highly excited nuclei with negligible compression and angular momentum. The ^{197}Au target produces significantly larger multiplicities of LCPs and IMFs than does $^{\mathrm{nat}}$Ag. Both the total observed charge and the total thermalized energy provide reliable gauges of the excitation energy distribution for the emitting source. For both systems, fragment emission appears to originate from a source in approximate kinetic equilibrium, for which Coulomb barriers are significantly lower than for nuclei at normal density. Qualitative agreement is found for the multiplicity data and the fragment kinetic energy spectra when compared with predictions of an intranuclear cascade or expanding emitting source calculation. In particular, the fragment spectra provide a compelling argument for nuclear expansion in light-ion-induced multifragmentation reactions—or for some mechanism involving significant perturbation of the nuclear Coulomb field at freezeout.

Funding for this experiment was provided by the U.S. Department of Energy, the Commissariat á l'Energie Atomique (France), the U.S. National Science Foundation, the National Science and Energy Research Council (Canada), NATO, and KBM Grant No. 0719/P3/93/04 (Poland).

[1] A. I. Warwick *et al.,* Phys. Rev. C **27**, 1083 (1983).
[2] S. J. Yennello *et al.,* Phys. Rev. Lett. **67**, 671 (1991); Phys. Rev. C **48**, 1092 (1993).
[3] J. Hubele *et al.,* Z. Phys. A **340**, 263 (1991).
[4] J. Natowitz *et al.,* Nucl. Phys. **A538**, 263c (1992).
[5] J. Peter *et al.,* Nucl. Phys. **A538**, 75c (1992).
[6] D. R. Bowman *et al.,* Phys. Rev. Lett. **67**, 1527 (1991); Phys. Rev. C **46**, 1834 (1992).
[7] W. G. Lynch, Annu. Rev. Nucl. Part. Sci. **37**, 439 (1987); L. G. Moretto and G. J. Wozniak, *ibid.* **43**, 379 (1993).
[8] R. T. deSouza *et al.,* Phys. Lett. B **268**, 6 (1991).
[9] K. Kwiatkowski *et al.,* Phys. Rev. C **49**, 1516 (1994).
[10] B. Li, R. De Angelis, and D. H. E. Gross, Phys. Lett. B **303**, 225 (1993).
[11] R. Wolfgang *et al.,* Phys. Rev. **103**, 394 (1956).
[12] J. Cugnon *et al.,* Nucl. Phys. **A379**, 553 (1982); **A462**, 751 (1987).
[13] K. Kwiatkowski *et al.,* Nucl. Instrum. Methods Phys. Res., Sect. A **353**, 212 (1994); (to be published).
[14] GEANT, CERN Program Library Report No. W5013, CERN, Geneva, Switzerland.
[15] L. Phair *et al.,* Phys. Lett. B **285**, 10 (1992); F. St. Laurent *et al.,* in *Proceedings of the International Workshop XII on Gross Properties and Nuclear Excitations,* edited by H. Feldmeier and W. Nörenberg (GSI, Darmstadt, Germany, 1994), p. 162.
[16] V. Lips *et al.,* Phys. Rev. Lett. **72**, 1604 (1994).
[17] D. H. E. Gross, Rep. Prog. Phys. **53**, 605 (1990).
[18] Y. Yariv and Z. Fraenkel, Phys. Rev. C **24**, 488 (1981).
[19] K. Kwiatkowski *et al.,* Phys. Lett. B **171**, 488 (1981).
[20] L. G. Moretto *et al.,* Nucl. Phys. **A247**, 211 (1975).
[21] W. A. Friedman, Phys. Rev. C **42**, 667 (1990).
[22] G. Fai and J. Randrup, Nucl. Phys. **A404**, 551 (1983); Comput. Phys. Commum. **42**, 385 (1986).